X-Disciplinarity

DOI: https://doi.org/10.63174/xdi.BEPO1073

Review

A Critical Review on Tensile Behavior and Johnson-Cook Constitutive Model Calibration of Wire Arc Additive Manufactured Materials

https://doi.org/10.63174/xdi.BEPO1073

Volume 2 Issue 2

Received: 13 May 2026

Accepted: 17 May 2026

Published: 18 May 2026

Open Access

Xin Liu[1, 2, 3, *]

Abstract: Wire arc additive manufacturing (WAAM) has emerged as a key near-net-shape fabrication route for large-scale aerospace metallic components, offering deposition rates of 3-10 kg/h and material utilization exceeding 90%. However, the non-equilibrium microstructures formed under repeated WAAM thermal cycling — comprising coarse columnar grains, heterogeneous Laves phase, Widmanstatten lamellar alpha, and gradient in-situ aging precipitates — render the mechanical behavior of as-deposited materials fundamentally distinct from wrought counterparts. This disparity gives rise to a systematic 'parameter transplantation fallacy' in engineering simulations that rely on Johnson-Cook (JC) constitutive parameters calibrated from forged stock. The present review systematically examines 69 representative studies published between 2009 and 2026, covering three representative WAAM structural materials: Inconel 718 (IN718), Ti-6Al-4V (TC4), and 18Ni300 maraging steel (18Ni300). A causal framework linking microstructure formation, tensile behavior, and JC calibration is established. Methodologically, this review proposes a new anisotropy classification taxonomy — texture-precipitate coupling type (IN718), grain boundary-texture type (TC4), and phase distribution-thermal history type (18Ni300) — and builds a cross-material three-tier error priority framework quantifying state-jump error, anisotropy error, and model calibration error. Key findings are: (i) classical JC models exhibit systematic prediction errors of 10-30% for WAAM materials at high strain rates (>1000 s^{-1}) and elevated temperatures (>600 °C); (ii) for WAAM IN718, the state-jump error (~42%) far exceeds the anisotropy error (~14%) and model error (<2%), establishing as-deposited-specific parameter databases as the highest-priority research task; (iii) all five JC parameters remain entirely uncharacterized for WAAM as-deposited 18Ni300, representing the most critical knowledge gap in the field. A research roadmap with specific experimental matrices is proposed for near-, mid-, and long-term research directions.

1. Introduction

The global aerospace manufacturing industry is undergoing a profound transformation from weight-reduction-driven structural optimization toward material-process integrated design paradigms. Wire arc additive manufacturing (WAAM) has demonstrated significant advantages in the near-net-shape fabrication of large-scale titanium alloy frames, nickel-based superalloy blisks, and ultra-high-strength steel structural components, owing to its deposition rates of 3-10 kg/h and material utilization exceeding 90% [1-4]. Das et al. [5] highlighted that the synergistic optimization of process, microstructure, properties, and simulation constitutes the core challenge in advancing WAAM toward industrial application. As WAAM components progressively enter service under extreme conditions including high-velocity impact, high-temperature creep, and cyclic fatigue, the accurate description of dynamic constitutive behavior has become increasingly critical [6].

The Johnson-Cook (JC) constitutive model, proposed in 1983 [1], has long served as the dominant engineering framework for describing large-deformation behavior of metallic materials, owing to its compact multiplicative form and physically interpretable parameters (quasi-static yield stress A, strain hardening B/n, strain rate sensitivity C, thermal softening m) [7]. However, a structurally important contradiction has been progressively overlooked: the vast majority of JC parameter databases originate from wrought or cast materials, while the distinctive microstructural features of WAAM materials — strong columnar grain texture and interdendritic Laves phase segregation (IN718), Widmanstatten lamellar alpha (TC4), and gradient in-situ aging precipitates (18Ni300, a grade of 18% Ni maraging steel) — give rise to fundamentally different strain hardening, strain-rate sensitivity, and thermal softening behavior compared to conventionally manufactured counterparts [8-10]. Directly transplanting wrought JC parameters to WAAM component simulations introduces errors reaching 10-30% at high strain rates [9,11], a 'parameter transplantation fallacy' that poses increasingly severe challenges to simulation fidelity.

The existing literature exhibits three systematic deficiencies. First, while Eisseler et al. [12] and Liang et al. [13] demonstrated that the directional A parameter discrepancy of 18Ni300 reaches 13.7%, studies providing

[1] School of Mechanical and Electronic Engineering, Shandong Agriculture and Engineering University, Jinan 250100, Shandong Province, PR China
[2] School of Mechanical Engineering, Universiti Sains Malaysia, 14300 Nibong Tebal, Pulau Pinang, Malaysia.
[3] Hongdian (Shandong) Digital Technology Co., Ltd, Jinan, Shandong Province, 250199, China.
[*] Corresponding Author: liux951127@163.com

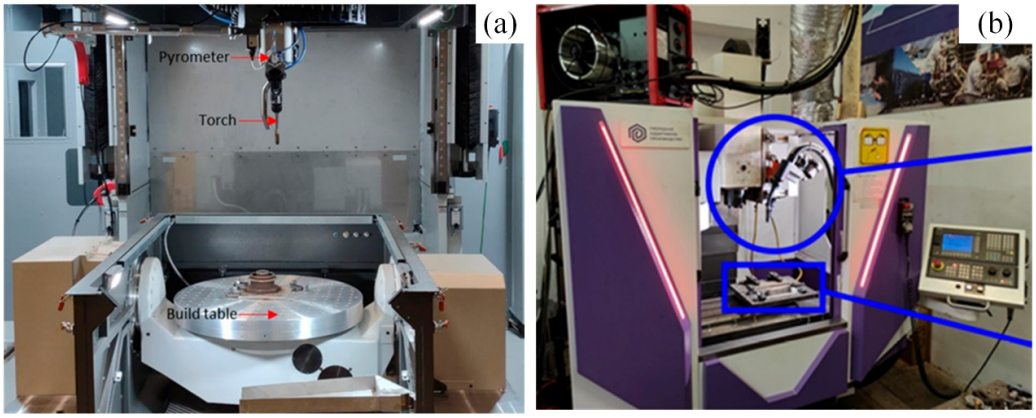

Figure 1. WAAM process setups and fabricated components. (a) Wire-arc DED system (b) CMT-based WAAM system. Reprinted from: (a) [16]; (b) [4].

directional (DD and SD) JC parameter sets for WAAM materials account for less than 5% of the published work, creating a structural void that propagates directional simulation errors. Second, although directional property differences (YS gap of 10-25%) are well documented for WAAM materials [8,10,11], most JC calibration studies still adopt an isotropic assumption. Third, no JC parameters have been reported for WAAM as-deposited 18Ni300 maraging steel [12-14]. Existing WAAM reviews (e.g., Das et al. [5]) focus primarily on process-defect-property relationships with limited depth on constitutive modeling; available JC calibration reviews (e.g., Gambirasio and Rizzi [7]) target wrought materials without systematically addressing the microstructural differences introduced by AM processes. The present review is the first to establish a causal analytical framework linking microstructure, anisotropy, and JC calibration reliability across three representative WAAM materials, filling this interdisciplinary gap. This review covers 69 representative publications spanning 2009-2026, organized along a causal logic of microstructure-to-tensile-behavior-to-JC-calibration. A new anisotropy taxonomy is proposed and a cross-material error priority evaluation framework is established, with the aim of providing systematic guidance for constitutive modeling of WAAM components.

2. As-deposited Microstructure and Tensile Behavior of WAAM Materials

2.1. WAAM Process Classification and Thermal Characteristics

WAAM employs an electric arc as the heat source and metallic wire as the feedstock, building three-dimensional structures through successive layer deposition. The process is broadly classified into three categories based on heat source type: gas metal arc welding (GMAW), gas tungsten arc welding (GTAW), and plasma arc welding (PAW). The cold metal transfer (CMT) variant, employing a specialized CMT torch with mechanical wire retraction, offers significantly reduced heat input and has gained widespread adoption for depositing high-performance alloys [2-4]. Das et al. [5] provided a systematic comparison of these processes in terms of deposition rate, heat input control, and material compatibility. The high-pressure inter-layer rolling technique developed by Colegrove et al. [15] demonstrated that compressive rolling between deposition passes substantially improves residual stress distribution and mechanical property uniformity, representing a landmark post-processing approach for WAAM. **Figure. 1** shows two representative WAAM equipment configurations. **Figure. 1** (a) is a wire-arc DED system illustrating the general torch-and-wire setup; **Figure. 1** (b) is a CMT-based WAAM system, whose mechanical wire retraction substantially reduces heat input compared to conventional GMAW, making it widely adopted for high-performance alloys such as IN718 and TC4.

The defining thermal characteristic of WAAM is the inter-layer cyclic thermal effect: each deposited layer undergoes repeated rapid heating-cooling cycles during subsequent layer deposition, with cooling rates in the range of 10-100 K/s — intermediate between casting (<1 K/s) and laser powder bed fusion (LPBF, 10^4-10^6 K/s) [6]. This distinctive thermal history directly shapes the phase transformation pathways, grain morphologies, and precipitate distributions of each material system, constituting the physical root cause of the systematic differences between WAAM material behavior and that of conventional manufacturing counterparts — and the deepest reason why wrought JC parameters cannot be directly transplanted to WAAM simulations.

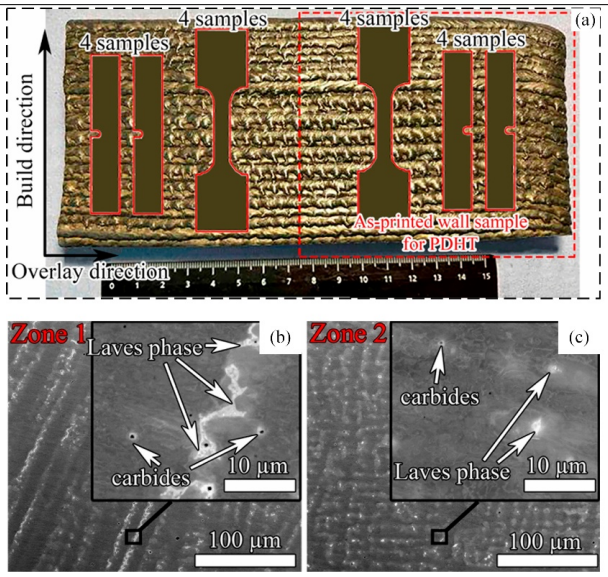

Figure 2. Tensile sample extraction and position-dependent microstructure of WAAM IN718. Reprinted from: (a-c) [11].

2.2. WAAM Inconel 718: Microstructure and Tensile Behavior

2.2.1. As-deposited Microstructure

The macrostructure of WAAM IN 718 (Inconel 718 fabricated by WAAM method) is characterized by epitaxially grown coarse columnar gamma-austenite grains with aspect ratios reaching 5:1 to 10:1, forming a strong <001> fiber texture [17]. Niobium enrichment in interdendritic regions drives the preferential precipitation of Laves phase ($(Ni,Fe,Cr)_2(Nb,Mo,Ti)$); the resulting Laves phase volume fraction in WAAM IN718 reaches 3–8%, far exceeding that typically observed in wrought IN718 (<1%) [10,17]. Tolcha et al. [18] revealed that the long-range diffusion kinetics of Nb directly governs the competitive precipitation pathway between Laves phase and the strengthening phase gamma-prime-prime (Ni_3Nb, D022 structure), providing the microstructural theoretical basis for heat treatment optimization. Popovich et al. [19] demonstrated that controlled thermal input gradients during deposition can engineer position-dependent textures and anisotropy in functionally graded IN718 components, offering a process-level strategy for actively tailoring IN718 anisotropy. **Figure 2** illustrates representative tensile specimen extraction layouts and position-dependent microstructural gradients in WAAM IN718, directly corroborating the build-height dependent property variations described in this section.

2.2.2. Tensile Behavior and Anisotropy

The above microstructural characteristics manifest as two directly quantifiable effects in macroscopic tensile behavior. First, the strength step-change effect: Laves phase consumes Nb and suppresses gamma-prime-prime precipitation, reducing the as-deposited yield strength (YS) to merely 420-630 MPa with ultimate tensile strength (UTS) in the range of 640-900 MPa, while elongation can reach 20-35% [10,20,21]. Following an improved solution annealing and

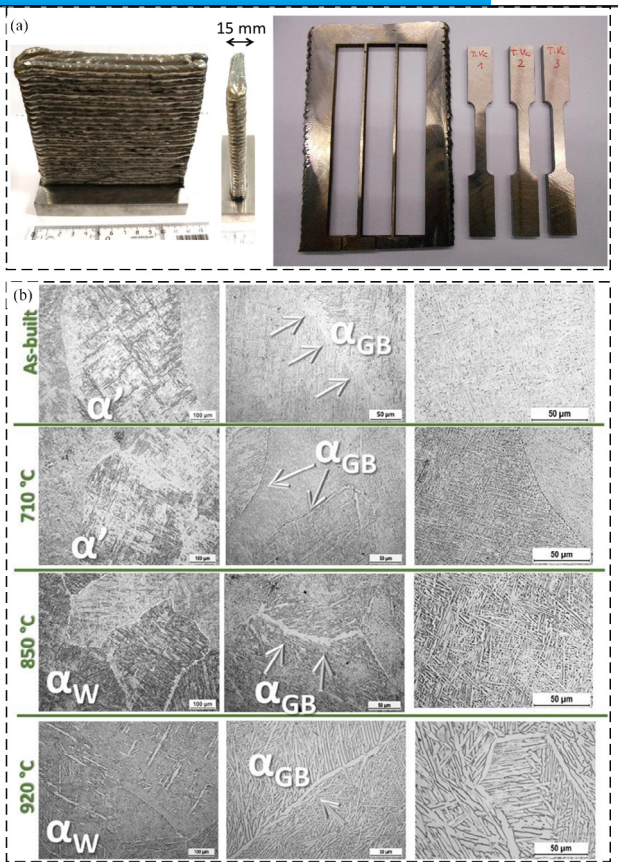

Figure 3. (a) Manufactured WAAM walls and Tensile specimens; (b) Evolution of the microstructures in the as-built state. Reprinted from: (a-b) [3].

double-step aging heat treatment (MHT), YS rises sharply to 1000-1100 MPa and UTS reaches 1200-1360 MPa, with elongation decreasing to 15-25% [10,22]. This step-change (delta YS > 600 MPa) is the largest heat treatment effect among the three material systems reviewed, physically arising from the coupled evolution of Laves phase dissolution and gamma-prime-prime precipitate volume fraction [23]. Smetannikov et al. [24] showed that inter-pass forging combined with heat treatment can achieve wrought-comparable strength without conventional forging operations, providing a novel pathway for high-performance near-net-shape WAAM IN718 components.

Second, the high-temperature instability effect: Song et al. [25] identified pronounced Portevin-Le Chatelier (PLC) serrated yielding in WAAM IN718 across 400-800 °C, attributable to dynamic strain aging (DSA) through solute Nb/Mo atom interactions with moving dislocations. The local Nb concentration in WAAM IN718 is 2-3 times higher than in wrought material due to dendritic segregation, expanding the PLC activation window from 600-700 °C (wrought) to 400-800 °C (WAAM) [9,25]. James et al. [26] systematically quantified the property degradation of WAAM IN718 at 538 °C, while Bhujangrao et al. [27] compared the high-temperature performance evolution between WAAM IN718 and wrought counterparts, jointly revealing the mechanism by which Laves phase induces brittle fracture at elevated temperatures. This high-temperature instability constitutes a non-linear behavior that the monotonic thermal softening term of classical JC cannot capture, directly forming the physical basis for the fourth category of systematic error discussed in Section 3.

Regarding anisotropy, IN718 exhibits a 'dual-dimensional anisotropy' — simultaneous differences in both yield strength (5-15%) and elongation (5-10 percentage points) [10,17]. Seow et al. [10] revealed that as-deposited anisotropy is relatively weak (BD-WA YS difference approximately 25 MPa), further diminishing after MHT. Zhang et al. [22,28] demonstrated that 75 kN inter-layer cold rolling induces dynamic recrystallization, transforming columnar grains to equiaxed, achieving post-HT strength exceeding AMS 5662 wrought specification (UTS > 1350 MPa) with anisotropy nearly eliminated. Alonso et al. [29] confirmed from a machinability perspective that heat treatment dramatically improves microstructural homogeneity, illustrating that anisotropy control effects can be verified across multiple engineering metrics. This dual-dimensional anisotropy implies that both A and n parameters require direction-specific calibration in JC modeling, making IN718 the most comprehensively affected material system among the three reviewed.

2.3. WAAM Ti-6Al-4V: Microstructure and Tensile Behavior

2.3.1. As-deposited Microstructure

The solidification structure of WAAM TC4 is dominated by coarse columnar prior-beta grains that epitaxially grow across multiple deposited layers [30,31]. On cooling, the beta-to-alpha transformation produces Widmanstatten lamellar α+β structures within the columnar beta grains, governed by the Burgers orientation relationship [32]. Ji et al. [33] demonstrated that inter-layer thermal cycling additionally induces banding — periodic coarsening of alpha lamellae in heat-affected zones — causing hardness fluctuations of approximately +/- 30 MPa, a characteristic manifestation of microstructural inhomogeneity in WAAM TC4. Grain boundary alpha (GB-alpha), forming as a continuous film along the build direction (covering > 70% of grain boundary area [8]), serves as the critical microscale origin of tensile anisotropy in subsequent mechanical testing. **Figure. 3** documents WAAM wall fabrication and the resulting as-built microstructure. **Figure. 3** (a) shows the deposited walls and extracted tensile specimens, illustrating the extraction strategy. **Figure. 3** (b) reveals the as-built grain morphology and phase distribution, which form the microstructural basis for the direction-dependent tensile behavior discussed in this section.

2.3.2. Tensile Behavior and Anisotropy

In contrast to the dual-dimensional anisotropy of IN718, TC4 anisotropy is predominantly concentrated in the elongation dimension. Carroll et al. [8] demonstrated that longitudinal and transverse elongations of DED TC4 are 11% and 14%, respectively, while UTS is approximately 1060 MPa in both directions, comparable to wrought specifications. GB-alpha forming as a continuous film (covering > 70% of grain boundary area [8]) acts as a preferential crack propagation pathway under longitudinal tensile loading, resulting in approximately 3 percentage point lower elongation in the build direction while strength difference remains < 5%. Colegrove et al. [15] showed that high-pressure inter-layer rolling disrupts GB-alpha continuity, reducing TC4 elongation anisotropy from ~3 percentage points to < 1 percentage point, providing direct experimental evidence for the causal relationship between GB-alpha continuity and elongation anisotropy.

Process-microstructure-property sensitivity is particularly pronounced for TC4. Brandl et al. [30] and Szost et al. [31] demonstrated that WAAM produces coarser alpha lamellae (width ~1-3 um) due to its slower cooling rates (10-100 K/s), yielding slightly lower room-temperature strength than LPBF but relatively superior fracture toughness. Wang et al. [34] showed that TC4/TC11 functionally graded WAAM structures achieve UTS = 980 MPa and elongation = 13.8% after solution and aging treatment, introducing new constitutive modeling challenges for multi-alloy gradient components. Wu et al. [35] identified an accelerated softening inflection in WAAM TC4 at 500-600 °C, signaling the onset of alpha-to-beta phase transformation, while Kim et al. [36] confirmed that as-deposited TC4 exhibits high UTS (> 920 MPa) with elongation constrained by the Widmanstatten lamellar structure (~13%). The predominance of elongation over strength anisotropy in TC4 implies that A parameter directional sensitivity is lower than in IN718, while n and C directional differences merit greater attention — quantified further in the calibration review of Section 4.

2.4 WAAM 18Ni300 Maraging Steel: Microstructure and Tensile Behavior

2.4.1. As-deposited Microstructure

18Ni300 maraging steel forms a lath martensite matrix during WAAM deposition [37,38]. Inter-layer thermal cycling with local peak temperatures ranging from 300 to 400°C — a range reflecting the positional variability of thermal history across different deposition layers rather than a single discrete transformation temperature — induces in-situ aging of previously deposited layers, precipitating Ni3Mo and Ni3Ti intermetallics and producing heterogeneous dispersion strengthening [37,39]. Zhang et al. [40,41] demonstrated that reduced heat input suppresses the non-uniformity of inter-layer in-situ aging, improving the strength gradient along the build height. Osman et al. [42] confirmed that post-deposition solution annealing and aging effectively homogenizes the gradient aging effect and improves mechanical property consistency in additive-subtractive hybrid manufactured 18Ni300. Notably, elevated heat input conditions promote the formation of delta-ferrite inclusions (hardness differential ~100 HV), a WAAM-specific microstructural defect that adversely affects impact toughness [40,43]. **Figure. 4** shows the fracture characteristics of WAAM material at the microscale. **Figure. 4** (a) reveals a near-surface defect in the failure zone, a stress concentrator arising from the layer-by-layer solidification process. **Figure. 4** (b) is an SEM image of the

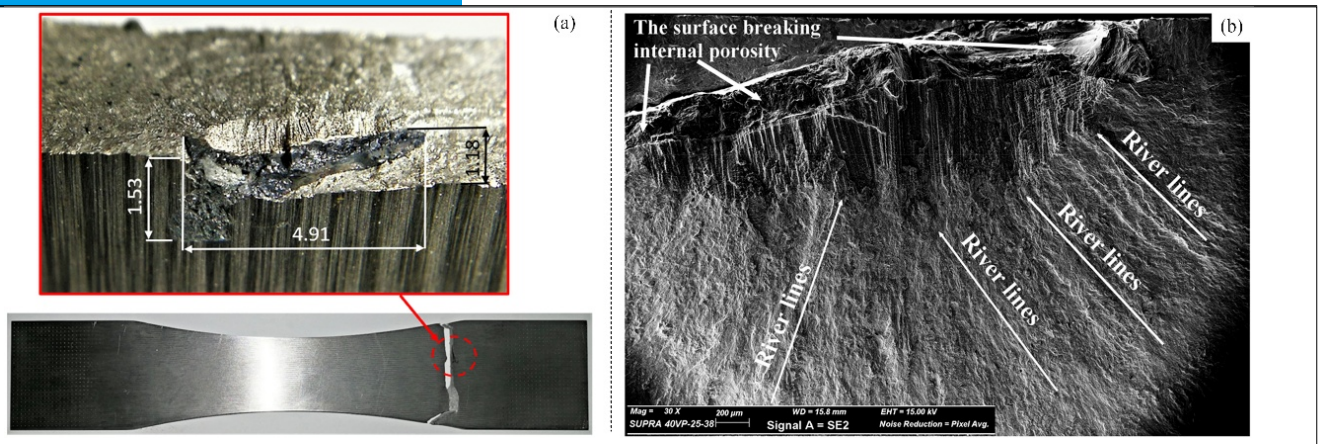

Figure 4. (a) Expanded view of the failure and the near-surface defect (b) SEM image of the critical location showing the multiple initiation sites. Reprinted from [46].

critical initiation region showing multiple crack initiation sites — a fracture mode distinct from the single-site initiation typical of wrought material and directly attributable to the heterogeneous as-deposited microstructure.

2.4.2. Tensile Behavior and Gradient Anisotropy

The tensile behavior of 18Ni300 differs fundamentally from the other two materials, characterized by ultra-high strength, low strain hardening, and gradient anisotropy. Mao et al. [44] reported that SLM 18Ni300 (a reference comparable to WAAM) achieves YS of 1762 MPa and UTS of ~1990 MPa after aging, with a strain hardening exponent n of only 0.2-0.3 and stress-strain curves saturating at approximately 3-5% strain [14,44]. This low-n characteristic poses unique challenges for JC parameter calibration: power-law fitting becomes extremely sensitive to the yield point definition when n approaches 0.2, with 0.2% versus 0.1% offset conditions yielding A values differing by ~50 MPa — the primary reason why 18Ni300 calibration is significantly more demanding than IN718 or TC4.

WAAM 18Ni300 exhibits a gradient anisotropy pattern distinct from the other two materials. Xu et al. [37] reported systematic strength gradients along the build height: bottom regions, having experienced longer thermal cycling, show higher hardness (HV 380-420) and UTS (> 1170 MPa) compared to top regions (HV 340-370, UTS ~1021 MPa), a gradient of approximately 15%. This implies that the primary direction of 18Ni300 anisotropy is 'along the build height' rather than the conventional 'parallel/perpendicular to build direction', making it the most distinctive anisotropy type among the three materials. Afkhami et al. [45] further revealed that build direction has limited influence on static strength (< 5%) but significantly affects cyclic fatigue performance, demonstrating that anisotropy characteristics are load-mode dependent. Pan et al. [39] showed that TRIP effects in 316L/18Ni300 layered heterogeneous structures increase composite elongation to 29%, providing a toughening design strategy for WAAM 18Ni300 components. Zhang et al. [41] and Peng et al. [46] provided experimental foundations for evaluating constitutive model applicability in dynamic fracture scenarios.

2.5. Comprehensive Comparison of Tensile Parameters

Table 1 systematically compiles the tensile property data for all three WAAM material systems. Cross-material analysis yields three regulatory conclusions that will be further quantified in the comparative analysis of Section 5:

- Rule 1 (Heat treatment strengthening inversely correlated with as-deposited precipitate content): IN718 achieves the largest heat treatment strengthening effect due to severely suppressed as-deposited gamma-prime-prime precipitation (YS gain > 600 MPa [10,22]); 18Ni300 shows moderate gains because in-situ aging already provides substantial as-deposited strength (YS gain ~400-500 MPa [42,44]); TC4 shows the smallest effect due to the absence of precipitation strengthening mechanisms (< 50 MPa [30,31]).
- Rule 2 (Material-dependent strength-ductility trade-off landscape): Heat-treated IN718 occupies the high-strength, low-ductility zone (UTS > 1200 MPa, EL < 25% [10,22]); TC4 occupies the intermediate-strength, moderate-ductility zone (UTS ~900-1100 MPa, EL 10-15% [8,30]); Aged 18Ni300 occupies the ultra-high-strength, near-zero-ductility zone (UTS > 1900 MPa, EL < 10% [13,44]). The current literature gap zone (1200-1900 MPa and EL > 15%) suggests potential breakthroughs in high-performance alloy design.
- Rule 3 (Divergence in anisotropy manifestation): IN718 anisotropy spans both YS (5-15%) and EL (5-10 percentage points) dimensions [10,17]; TC4 anisotropy is primarily expressed in EL (~3 percentage points) and is difficult to eliminate by conventional annealing [8,15]; 18Ni300 anisotropy is mainly a build-height strength gradient (~15% [37]) rather than in-plane directional variation — these three distinct types require different JC modeling and calibration strategies [12,13].

The systematic differences in tensile behavior among the three material systems fundamentally originate from their distinct strain hardening mechanisms, dislocation-second phase interactions, and anisotropic texture characteristics. These differences directly determine the descriptive capability boundaries of the Johnson-Cook constitutive model — Section 3 will trace how these microscale features propagate into systematic calibration errors

Table 1. Summary of tensile mechanical properties of WAAM and related AM materials.

No.	Reference	Material & State	UTS(MPa)	YS(MPa)	EL(%)	E(GPa)	Hardness	Data Type & Test Conditions
1	Seow et al. [10] Mater. Des. 2019	WAAM IN718, as-deposited BD direction	756	431	21.3	125	—	(1) Direct test | BD vs WA anisotropy weak
2	Seow et al. [10] Mater. Des. 2019	WAAM IN718, MHT state BD direction	1044	856	19.9	178	—	(1) Direct test | HT eliminates anisotropy
3	Xu X et al. [20] J. Manuf. Process. 2019	WAAM IN718 (CMT) as-deposited	827	482	32.9	—	275 HV	(1) Direct test | EL far exceeds PBF
4	Xi et al. [9] J. Manuf. Process. 2022	WAAM IN718, as-deposited Horizontal H / Vertical V	841/890	597/613	~33	—	—	(1) Direct test | Direction strength diff. <5%
5	Xi et al. [9] J. Manuf. Process. 2022	WAAM IN718, MHT Horizontal H / Vertical V	1249/1251	1070/1071	~21	—	—	(1) Direct test | HT eliminates anisotropy
6	Zhang T et al. [22] J. Alloys Compd. 2021	WAAM IN718, as-deposited	840.7	472.5	26.3	—	260 HV	(1) Direct test
7	Zhang T et al. [22] J. Alloys Compd. 2021	WAAM IN718 75kN rolling + HT	1357.3	1067.4	15.8	—	420 HV	(1) Direct test | Exceeds AMS5662 wrought spec.

8	James et al. [26] Sci. Rep. 2023	WAAM IN718, as-deposited RT / 538 degC	626/478	505/378	—	125	—	(2) Elevated-temp. test | Laves phase causes HT brittleness
9	James et al. [26] Sci. Rep. 2023	WAAM IN718, HT state RT / 538 degC	870/761	852/687	—	178	—	(2) Elevated-temp. test | HT improves HT toughness
10	Bhujangrao et al. [27] Crystals 2020	WAAM IN718, RT	684	621	6.5	—	—	(1) Direct test | EL lower than wrought (31%)
11	Mota et al. [38] Machines 2026	WLAM IN718, as-deposited horizontal	824	447	41	—	—	(1) Direct test | Low heat input, high EL
12	Mota et al. [38] Machines 2026	WLAM IN718, HT state	1057	853	25	—	—	(1) Direct test | SA + aging
13	Qi et al. [23] Metall. Trans. A 2009	LNSM IN718, as-built	904	552	8.4	—	—	(1) Direct test
14	Qi et al. [23] Metall. Trans. A 2009	LNSM IN718, STA state	1194	1007	16.0	—	—	(1) Direct test | Superior post-STA performance
15	Kishore et al. [47] Adv. Manuf. 2026	WAAM IN718, optimized	788	345	74.3	—	—	(1) Direct test | Extremely high EL via RSM
16	Carroll et al. [8] Acta Mater. 2015	DED Ti-6Al-4V Longitudinal L / Transverse T	~1060	—	11 / 14	—	—	(1) Direct test | EL anisotropic, strength comparable
17	Martina et al. [48] J. Manuf. Process. 2012	Plasma WAAM TC4 as-deposited	—	~860	~8	—	~330 HV	(1) Direct test | PAW process
18	Szost et al. [31] Mater. Des. 2016	WAAM Ti-6Al-4V as-deposited	~920	~785	~13	—	330 HV	(1) Direct test | Comparable to wrought
19	Brandl et al. [30] MSEA 2012	Wire-feed ALM TC4 as-deposited	—	~780	~10	—	—	(1) Direct test | Coarser lamellae, lower EL
20	Kim et al. [36] Sci. Rep. 2025	WAAM Ti-6Al-4V as-deposited	~1100	~970	~13	—	—	(1) Direct test | High UTS from lamellar strengthening
21	Zhou et al. [32] J. Mater. Res. Tech. 2024	WAAM-LDM Ti-6Al-4V	942	—	12.5	—	—	(1) Direct test | Good interface bonding
22	Wang J et al. [34] J. Manuf. Process. 2024	TC4/TC11 FGM Solution-aged state	980	—	13.8	—	—	(1) Direct test | Dual-wire gradient WAAM
23	Xu X et al. [37] Mater. Charact. 2018	WAAM 18Ni300, as-deposited XD/YD/ZD directions	1021-1172	—	8-12	—	340-380 HV	(1) Direct test | Height-gradient anisotropy
24	Pan et al. [39] MSEA 2023	WAAM 316L/18Ni300 laminated (18Ni300 side)	963	677	13.7	—	—	(1) Direct test | TRIP improves ductility
25	Zhang J et al. [40] MSEA 2023	WAAM 18Ni300, CMT	1271	—	19.7	—	—	(1) Direct test | Low HI improves homogeneity
26	Mao et al. [44] MSEA 2022	SLM 18Ni300, as-built	1245	1052	10.5	164	—	(1) Direct test | SLM reference
27	Mao et al. [44] MSEA 2022	SLM 18Ni300 Solution+ aging (STA)	1915	1762	5.0	179	54 HRC	(1) Direct test | Ni3Mo/Ni3Ti precipitation
28	Liang et al. [13] Materials 2024	SLM 18Ni300, 0-deg. SHPB dynamic	—	921(comp.)	—	—	46-48 HRC	(1) Direct dynamic test | Quasi-static dir. diff. <1%
29	Liang et al. [13] Materials 2024	SLM 18Ni300, 90-deg. SHPB dynamic	—	949(comp.)	—	—	46-48 HRC	(1) Direct dynamic test | Dynamic diff. 9.8%
30	Asala et al. [49] IJAMT 2019	WAAM ATI 718Plus as-deposited (SHPB)	—	632.5	—	—	—	(1) SHPB test | 1500-3500 s^{-1}
31	Kishor et al. [50] Eng. Fail. Anal. 2025	WAAM IN625 RT - horizontal	815	540	62.3	—	—	(1) Direct test | Note: IN625, not IN718
32	Kishor et al. [50] Eng. Fail. Anal. 2025	WAAM IN625 RT - vertical	735	475	60.6	—	—	(1) Direct test | Do not mix with IN718 data
33	Okuniewski et al. [51] Adv. Sci. Tech. 2026	WLMD 316L 0-deg. print direction	699	296	—	148	—	(1) Direct test | Significant E directional diff.
34	Okuniewski et al. [51] Adv. Sci. Tech. 2026	WLMD 316L 90-deg. print direction	594	372	—	186	—	(1) Direct test | YS diff. 26%
35	Osman et al. [42] Materials 2023	WAAM-SAM 18Ni300 HT state reference	—	—	—	—	~50 HRC	(3) Literature-cited | Additive-subtractive hybrid reference

Note: BD — build direction; WA — wall width direction; DD — deposition direction; SD — scanning direction; RT — room temperature; — indicates not reported in literature. Data source types: (1) Direct tensile measurement; (2) Elevated-temperature tensile measurement; (3) Literature-cited value. UTS and YS in MPa; E in GPa.

across the five JC parameters (A, B, n, C, m), establishing the analytical pathway from material microstructure to model limitations.

3. Johnson-Cook Constitutive Model Framework and Calibration Methods

3.1 Mathematical Framework and Physical Significance

Johnson and Cook (1983) proposed the following empirical multiplicative constitutive model [1]:

$$\sigma = (A + B\varepsilon^{n})(1 + C\ln\ \varepsilon^{*})(1 - T^{*m}) \quad (1)$$

where ε is the equivalent plastic strain; $\varepsilon^{*} = \varepsilon/\dot{\varepsilon}_0$ is the dimensionless strain rate (reference strain rate $\dot{\varepsilon}_0$ typically set to 10^{-3} s^{-1}); $T^{*} = (T - T_r)/(T_m - T_r)$ is the dimensionless temperature; A is the quasi-static yield stress at reference conditions; B and n are the strain hardening coefficient and exponent; C is the strain rate sensitivity coefficient; and m is the thermal softening exponent. The multiplicative form assumes independence among the three effects — simultaneously the source of the model's simplicity and engineering utility, and the root of its fundamental limitations [7].

Among the five parameters, the thermal softening exponent m has received the least attention in WAAM material research, yet its importance is no less than the others. Reported m values for wrought IN718 span 1.3-4.3, a wide scatter primarily attributable to additional softening from phase transformations at elevated temperatures, producing non-monotonic thermal softening behavior that a simple power-law temperature term cannot accurately capture [9,25]. WAAM TC4 shows m values of approximately 0.8-1.02, the most stable among the three systems, but with an accelerated softening inflection at 500-600 °C due to the onset of alpha-to-beta phase transformation [35,52]. The m parameter is entirely absent for all three WAAM material systems, with high-temperature SHPB testing challenges as the primary technical barrier — this represents the most severe single-parameter data gap in the field.

3.2. JC Parameter Calibration Methodology

- A, B, n parameters: Obtained by fitting true stress-true strain curves from quasi-static tests (10^{-3} to 10^{-1} s^{-1}). Gambirasio and Rizzi [7] showed through a systematic comparison of five strategies (LYS, TYS, RCOS, etc.) that the GOPTEPS approach, based on full-curve fitting (AL-6XN stainless steel: A = 256.87, B = 2511.9, n = 0.434), minimizes global error, though the optimal strategy varies by material.
- C parameter: Obtained from split Hopkinson pressure bar (SHPB) experiments (10^{2} to 10^{4} s^{-1}) at reference temperature. Critical note: adiabatic temperature rise (delta-T approximately 30-80 °C) generated during high-rate deformation in SHPB tests systematically underestimates C if uncorrected [53]. Zhu et al. [53] demonstrated an iterative correction that increased the C value of TC4 from 0.0197 to 0.035 (a 78% increase), a correction procedure applicable to all AM material C-parameter calibrations.
- m parameter: Obtained from high-temperature tensile or high-temperature SHPB tests at different temperatures, fitting the thermal softening term against T*. Technical challenges of high-temperature SHPB (radiative heat loss, bar oxidation) make m the least accurately calibrated of the three parameter groups. The high-temperature TC4 flow data provided by Lee and Lin [52] at 400-900 °C remains an essential reference for m-parameter calibration to this day.

Inverse identification offers an important alternative for AM materials where small-specimen SHPB preparation is technically challenging. Eisseler et al. [12] combined orthogonal cutting experiments with FEM simulation, minimizing cutting force residuals to inversely determine direction-dependent JC parameters for LPBF 18Ni300 and successfully quantified a 13.7% directional difference [12]. Multi-population genetic algorithms (MPGA) demonstrate superior global search capability over conventional least squares methods in inverse identification [54], and the five-strategy comparison by Gambirasio et al. [7] provides theoretical guidance for parameter set selection in different machining scenarios.

3.3. Sources and Magnitudes of Systematic Calibration Errors for WAAM Materials

Understanding how WAAM-specific microstructural features influence the range of JC parameter values is the critical bridge for interpreting calibration error sources. Regarding the strain hardening terms (A, B, n): Laves phase in IN718 impedes dislocation glide and elevates the initial work hardening rate (elevated B value), while locally Nb-depleted zones reduce gamma-prime-prime precipitation, systematically depressing A below aged-state values; the orientation consistency of Widmanstatten lamellae in TC4 constrains slip system activation diversity, making n (approximately 0.34-0.71) sensitive to lamellar orientation direction; the ultra-low n of 18Ni300 (~0.2) arises from the already high dislocation density (~10^{14} m^{-2}) in the lath martensite matrix, leaving minimal capacity for further work hardening [13,44].

Four categories of systematic errors arise when applying classical JC to WAAM materials, with differing magnitudes and dominant effects across the three material systems:

(1) Anisotropy error: A fundamental contradiction exists between JC's isotropic assumption and the directional dependence of WAAM materials. Quantitatively: 18Ni300 directional A difference ~13.7% [12,13]; IN718 directional A difference 5-15% [10,17]; TC4 directional C difference ~25% (from TC11 reference data [54]). IN718 anisotropy error spans the widest parameter range (both A and n affected); 18Ni300 shows the largest magnitude. (2) Adiabatic temperature rise error: Uncorrected adiabatic heating (ΔT ~30-80 °C) in SHPB tests systematically underestimates C; Zhu et al. [53] demonstrated ~78% underestimation for TC4; this error is universally present across all three material systems. (3) Strain hardening saturation error: Ultra-low n in 18Ni300 causes power-law fitting failure beyond 3-5% strain [14]; smaller in IN718 and TC4. (4) Phase transformation-induced error: Alpha-to-beta transformation in TC4 at elevated temperature, TRIP effect in 18Ni300, and DSA/PLC effect in IN718 all exceed the descriptive capacity of classical JC, with errors reaching 10-30% in the high-temperature regime [9,25,55].

This magnitude analysis yields an operationally significant engineering guideline: the dominant error source differs by material, and targeted improvements to JC modeling should reflect this material-specificity. For IN718, temperature-strain rate coupling correction at elevated temperatures should take priority; for TC4, adiabatic temperature rise correction and anisotropic parameterization are most critical; for 18Ni300, the strain hardening saturation problem and the establishment of as-deposited-specific parameter sets must be addressed first. Section 4 systematically reviews the progress and limitations of existing calibration work for each material system, organized around this error priority hierarchy.

4. JC Constitutive Calibration Progress by Material System

To facilitate the cross-material comparative analysis that follows, **Table 2** presents a comprehensive summary of Johnson–Cook constitutive model parameters reported for WAAM and related AM materials, encompassing all three representative material systems (IN718, TC4, and 18Ni300) across deposition states (as-deposited, stress-relieved, and heat-treated) and calibration methodologies. Each entry documents the five core JC parameters (A, B, n, C, m), applicable strain rate and temperature ranges, accuracy metrics, and data provenance. Entries marked with ★ represent the recommended parameter set with highest validated accuracy; --* denotes untested conditions; --† indicates tested but unreported results; and --‡ indicates conditions where the classical power-law hardening term is inapplicable. This table serves as the primary data foundation for the parameter scatter analysis in Section 4.1, the improvement strategy review in Section 4.2, and the calibration gap identification in Section 4.3.

4.1. Parameter Scatter and Applicability Boundary of Classical JC

Before evaluating classical JC applicability, a fundamental data quality issue must be acknowledged. Reported JC A-parameter values for IN718 span 473-1200 MPa (Table 2, entries 4-9; IN625 data [50] excluded, as IN625's A = 230 MPa reflects the lower precipitation strengthening level of a different alloy and must not be conflated with IN718), representing a ~2.5-fold scatter. This large scatter originates from three sources: material state (as-deposited vs. heat-treated, gap ~600 MPa [10,22]); test condition (quasi-static vs. high-temperature, gap ~350 MPa [11,56,57]); and calibration method (direct testing vs. inverse identification, gap ~100-200 MPa [7,12]). For TC4, wrought JC A values range from 862 to 1000 MPa (**Table 2**, entries 2, 15), a ~16% scatter attributable to microstructural state and test temperature [52,54]. For 18Ni300, A values range from 700 to 1000 MPa (**Table 2**, entries 17-21), with directional difference ~13.7% and state difference ~25% [12,13,58]. This scatter means that engineers invoking JC parameters must rigorously verify calibration conditions, as errors can far exceed the model's own fitting accuracy — the fundamental motivation for establishing WAAM-specific parameter sets.

Using a unified accuracy criterion (AARE < 5% = 'engineering-applicable'; 5-10% = 'use with caution'; > 10% = 'requires improvement' [7,9]), Fan et al. [11] explicitly quantified classical JC applicability for IN718: AARE reaching 27.34%, with primary errors concentrated in the high-strain-rate regime (dislocation pile-up effects) and elevated-temperature regime (PLC effect). Grzesik et al. [56] showed that the M2 model achieves only 1-2%

Table 2. Summary of Johnson-Cook constitutive model parameters for WAAM and related AM materials.

No.	Reference	Material & State	A (MPa)	B (MPa)	n	C	m	Accuracy Metric	Calibration Method	Data Type / ★
1	Johnson & Cook [1] 1983	OFHC copper (wrought) original model anchor	90	292	0.31	0.025	1.09	Standard validation	Tension+torsion	Anchor reference
2	Johnson & Cook [1] 1983	Ti-6Al-4V (wrought) original model anchor	862	331	0.34	0.012	0.80	Standard validation	Tension+torsion	Wrought baseline; not for WAAM
3	Johnson & Cook [1] 1983	4340 steel (wrought) methodological basis	792	510	0.26	0.014	1.03	Standard validation	Tension+torsion	Methodological basis
4	Fan et al. [11] 2022 IMechE	Inconel 718, wrought dislocation-pile-up mod. JC	758	981	0.50	0.010	1.625	AARE 3.72% vs. classical 27.34%	SHPB dynamic compression	Direct meas.; dislocation correction
5	Grzesik et al. [56] 2017 JMEP	Inconel 718, M2 model machining-scene optimized	1012	511	0.396	0.0271	4.331	Cutting force err. 1-2% 500-600 degC verified	SHPB + high-temp. tension	Direct meas.; machining context
6	Aslam et al. [57] 2020 JPC	IN718, aerospace grade bird-strike simulation	1200	1140	0.65	0.006	1.3	Bird-strike sim. verified	(3) Literature-cited	(3) Cited value; use caution for WAAM
7 ★	**Xi et al. [9] 2022 JMP**	**WAAM IN718, MHT state T-strain rate coupling mod. JC**	**1025.4**	**1066.2**	**0.87**	**1.65e-5**	**1.06**	**AARE<1.71% ★ HT regime verified**	**SHPB + multi-T tension**	**Direct meas.; WAAM HT state ★ BEST**
8	Raj et al. [61] 2024 PAM	DED IN718, micro-rolling FEM simulation params.	473	564.24	0.368	--†	1.61	FEM warpage verified	(3) FEM process sim.	(3) Cited value; process sim.
9	Asala et al. [49] 2019 IJAMT	WAAM ATI 718Plus as-deposited, mod. JC	632.5	1721.31	0.655	C1=0.0658	--*	R=0.9764 AAE=4.26%	SHPB 1500-3500 s^{-1}	Direct meas.; T-rate coupling terms
10	Kishor et al. [50] 2025 EFA	WAAM IN625 (400 degC ref.; note: not IN718)	230	99.48	1.60	0.26	0.523	MAE=2.78%	SHPB + high-temp. tension	Direct meas.; IN625 system; do not mix
11	Lee & Lin [52] 1997 JMPT	Ti-6Al-4V, wrought m calibration baseline data	970(400 degC)	--†	--†	--†	--†	HT baseline data	High-temp. tension	Direct meas.; m-param. reference
12 ★	**Tian et al. [54] 2022 Materials**	**WAAM TC11, as-deposited SD direction, mod. JC**	**1046.6**	**979.4**	**0.707**	**0.0146**	**--***	**R^2>0.99 MPGA opt. ★**	**SHPB 0.001-4000 s^{-1}**	**Direct meas.; only WAAM Ti JC ★ BEST**
13	Zhu et al. [53] 2021 MTC	Ti6Al4V, wrought SHPB adiabatic rise corr.	—	—	—	0.035(corrected)	—	Machining accuracy improved	SHPB iterative corr.	Corrected; orig. C=0.0197 underest. 78%
14	Muiruri et al. [55] 2022 Materials	LPBF Ti6Al4V(ELI) high-rate SHPB verified	920	380	0.578	0.042	0.633	SHPB err. <4%	LPBF+SHPB+VUMAT	Direct meas.; high-strain regime needs corr.
15	Mathews et al. [62] 2024 Procedia	WAAM Ti-6Al-4V thermomechanical sim.	1000	780	0.47	--†	1.02	Thermo-mech. FEM verified	(3) FEM process sim.	(3) Cited value; process sim.
16	Fu et al. [59] 2020 STWJ	18Ni maraging steel, wrought failure params. D1-D5	~1000	--†	--†	--†	--*	R^2=0.99	SHTB dynamic tension	Direct meas.; D1=0.088 D5=2.912
17 ★	**Eisseler et al. [12] 2022 Materials**	**LPBF 18Ni300, 0-deg. inverse-identified JC**	**816.72**	**163.85**	**0.2166**	**--†**	**--†**	**Cutting force diff. 7.56% dir. diff. 13.7% ★**	**Inverse FEM identification**	**Inverse ID; directional ★ RECOMMENDED**
18	Eisseler et al. [12] 2022 Materials	LPBF 18Ni300, 90-deg. inverse-identified JC	705.0	179.96	0.213	--†	--†	Compare with 0-deg.	Inverse FEM identification	Inverse ID; compare with entry 17
19 ★	**Liang et al. [13] 2024 Materials**	**SLM 18Ni300, 0-deg. nonlinear-C mod. JC**	**921**	**112**	**0.303**	**0.0083**	**--***	**Dynamic diff. 9.8% ★**	**SHPB quasi-static+dynamic**	**Direct meas.; directional ★ RECOMMENDED**
20	Liang et al. [13] 2024 Materials	SLM 18Ni300, 90-deg. nonlinear-C mod. JC	949	100	0.209	0.0102	--*	Compare with 0-deg.	SHPB quasi-static+dynamic	Direct meas.; compare with entry 19

21	Tang et al. [58] 2026 JMP	18Ni300, solution state machining sim. ref. params.	1000	510	0.26	0.05	1.03	SAM sim. err.<15%	(3) Literature-cited	(3) Cited; not WAAM as-deposited; use caution
22	Silva et al. [14] 2021 JMMP	AM 18Ni300 Swift-Voce replaces JC	--‡	--‡	--‡	--‡	--‡	Near-ideal plastic; JC fails	Orthogonal cutting test	ddagger method not applicable; PL hardening fails
23	Behseresht & Park [63] 2025 Metals	Mild steel WAAM process sim. JC	363	792.7	0.5756	0.0054	1.6456	Warpage FEM err.<10%	WAAM process sim.	(3) Cited; JC vs. isotropic comparison
24	Okuniewski et al. [51] 2026 ASTJ	WLMD 316L 0-deg. printing	295	827	0.25	--†	--†	Print direction effect marked	WLMD + tension	Direct meas.; n diff. 169%
25	Okuniewski et al. [51] 2026 ASTJ	WLMD 316L 90-deg. printing	372	983	0.671	--†	--†	A diff. 26%	WLMD + tension	Direct meas.
26	Gambirasio & Rizzi [7] 2014 MSEA	AL-6XN stainless steel GOPTEPS strategy	256.87	2511.9	0.434	0.004	0.499	5-strategy error comparison	Multi-algorithm comparison	Direct meas.; calibration methodology basis
27	Zhang S et al. [64] 2024 Machines	06Cr18Ni11Ti weld grinding sim.	270	1179.99	0.890	0.085	0.493	Grinding force err. 13.8%	GTAW weld + SHPB	Direct meas.; weld microstructure specific

Note: ★ = recommended parameter set (highest accuracy, multi-condition validated); --* = not tested; --† = tested but not reported; --‡ = method not applicable (power-law hardening term fails for near-ideal-plastic behavior). Accuracy metrics: AARE = average absolute relative error; R = correlation coefficient; MAE = mean absolute error; AAE = average absolute error percentage.

error in machining scenarios (500-600 °C) but cannot be extrapolated to room-temperature large-deformation conditions. Muiruri et al. [55] identified an inherent theoretical flaw of classical JC at high strain levels (> 0.5): unbounded stress increase, with SHPB simulation errors exceeding 15% in the high-strain regime. Silva et al. [14] identified the fundamental failure of the classical JC power-law hardening term for the near-ideal-plastic behavior of 18Ni300: with n approximately 0.2, the power function converges too rapidly at 3-5% strain, underestimating stress by approximately 10-15%.

4.2. Three Categories of Improvement Strategies (Cross-material Review)

4.2.1. Strategy A: Temperature-Strain Rate Coupling Correction — IN718-centric

Temperature-strain rate coupling correction overcomes the independence assumption of the classical JC multiplicative form by introducing a coupling function $F(T^*, \varepsilon^*)$, and represents the primary approach for reducing elevated-temperature PLC-effect errors in IN718. Xi et al. [9] established the most systematic modified JC calibration work to date for WAAM IN718 in the heat-treated state: introducing the coupling correction function compressed prediction AARE from > 10% to < 1.71% (**Table 2**, entry 7, recommended parameter set: A = 1025.4, B = 1066.2, n = 0.87, C = 1.65e-5, m = 1.06) [9]. Fan et al. [11] employed dislocation pile-up theory correction to reduce IN718 wrought prediction error from 27.34% to 3.72% (Table 2, entry 4: A = 758, B = 981, n = 0.50), revealing the importance of the dislocation-obstacle interaction term absent from classical JC.

This strategy is equally applicable to TC4: Tian et al. [54] found that TC4 thermal softening and strain rate hardening exhibit coupling effects at intermediate-to-elevated temperatures (400-600 °C), causing classical JC to systematically overestimate flow stress by ~8%. Lee and Lin [52] provide TC4 high-temperature experimental data (**Table 2**, entry 11) that, although from wrought material, remain the primary reference for TC4 m-parameter calibration and provide a baseline for comparing thermal softening differences between WAAM TC4 and wrought stock. Asala et al. [49] demonstrated for WAAM ATI 718Plus (**Table 2**, entry 9, R = 0.9764) that a modified JC with coupling correction outperforms the Arrhenius model, providing an important cross-reference for constitutive modeling of WAAM 718-series alloys [49].

4.2.2. Strategy B: Nonlinear Strain Rate and Adiabatic Temperature Rise Correction — TC4-centric

Nonlinear strain rate correction addresses the failure of the classical JC linear $C \cdot \ln(\varepsilon)$ assumption at high strain rates (> 500 s^{-1}) by introducing piecewise functions or nonlinear terms into the C parameter. Tian et al. [54] performed the only complete JC calibration to date specifically for WAAM titanium alloy as-deposited state (TC11): spanning 0.001-4000 s^{-1}, a nonlinear strain rate transition at ~500 s^{-1} was identified and a modified JC incorporating this transition was proposed (**Table 2**, entry 12, recommended: A = 1046.6, B = 979.4, n = 0.707, C = 0.0146), calibrated via MPGA with $R^2 > 0.99$ [54]. The compositional difference between TC11 and TC4 (quasi-static YS difference ~120-180 MPa [30,54]) precludes direct parameter transplantation, but the methodology is directly transferable.

Although SHPB adiabatic temperature rise correction was first systematically studied in TC4, its physical basis — adiabatic process thermodynamics at high strain rates — applies equally to IN718, TC4, and 18Ni300, making it a universal calibration procedure improvement for all AM materials. Zhu et al. [53] demonstrated that their iterative correction scheme increased TC4's C value from 0.0197 to 0.035 (78% increase), substantially improving machining force prediction accuracy (**Table 2**, entry 13). Muiruri et al. [55] integrated microstructure-variable-based VUMAT corrections in LPBF Ti6Al4V, compressing SHPB simulation errors to < 4% (**Table 2**, entry 14), further demonstrating the potential of microstructure-informed corrections for AM material JC accuracy [55].

4.2.3. Strategy C: Inverse Identification and Anisotropic Parameterization — 18Ni300-centric

Inverse identification minimizes the residual between FEM simulation and experimental measurements to back-calculate JC parameters, effectively circumventing the technical challenge of small-specimen SHPB preparation for AM materials, while naturally accommodating directional parameter sets. Eisseler et al. [12] pioneered combining orthogonal cutting experiments with FEM simulation, successfully distinguishing 0° (**Table 2**, entry 17: A = 816.72, B = 163.85, n = 0.2166, recommended) and 90° (**Table 2**, entry 18: A = 705, B = 179.96, n = 0.213) directional parameters for LPBF 18Ni300, with cutting force prediction disagreement of 7.56% [12]. Liang et al. [13] provided verification through direct quasi-static and SHPB testing: modified JC for SLM 18Ni300 distinguished 0° (Table 2, entry 19: A = 921, n = 0.303, recommended) and 90° (**Table 2**, entry 20: A = 949, n = 0.209) parameters, with dynamic yield strength directional difference of 9.8% [13]. The mutual corroboration of two independent methods enhances the reliability of directional JC parameters for 18Ni300. This strategy is directly applicable to IN718 and TC4 anisotropy calibration, but no study has yet applied it to the WAAM as-deposited state of these materials — a critical methodological extension opportunity for near-term research.

4.3. WAAM-specific Calibration Challenges and Current Gaps

Beyond improvement strategy discussions, WAAM processing introduces three categories of calibration challenges not previously encountered in traditional material calibration, collectively constituting the primary barriers to engineering application.

Challenge 1 (As-deposited to heat-treated state parameter jump): WAAM IN718 undergoes a ~42% parameter jump from as-deposited state (A approximately 597 MPa) to MHT heat-treated state (A approximately 1025 MPa) [9,10]; 18Ni300 shows ~20% jump from solution state (A approximately

758 MPa [58]) to aged state (A > 900 MPa [13,44]). This implies that a single component requires entirely different JC parameter sets at different processing stages — yet only Xi et al. [9] have systematically calibrated IN718 in the heat-treated state, while as-deposited parameters remain entirely absent.

Challenge 2 (Position-dependent gradient parameterization requirement): 18Ni300 WAAM components show ~15% strength gradient from bottom to top (A difference ~150 MPa [37]); TC4 inter-layer banding causes hardness fluctuations of approximately +/- 30 MPa [33]. Both imply that a single uniform parameter set cannot accurately describe mechanical behavior across the entire component, necessitating position-dependent JC parameter distribution methods. This challenge has not been resolved in any existing calibration study and represents an important frontier for refined WAAM constitutive modeling.

Challenge 3 (Complete absence of WAAM as-deposited 18Ni300 JC data): Failure parameters from wrought 18Ni300 (D1-D5, Fu et al. [59]), solution-state reference values (A = 1000, B = 510, n = 0.26, Tang et al. [58]), and machining-cited values (Yao et al. [60,61]) are all non-WAAM as-deposited measured results. Sohail and Reddy [43] indirectly confirmed that significantly different heat treatment states of 18Ni300 produce markedly different machining responses, implying that the magnitude of parameter transplantation errors cannot be estimated, making the establishment of WAAM as-deposited-specific parameter sets the most urgent task.

The three calibration challenges collectively expose a core disconnection in current WAAM constitutive research: while improvement of JC functional forms has accumulated modest progress, the establishment of as-deposited-specific parameter sets and resolution of anisotropic parameterization remain severely lagging. Section 5 will quantify the magnitude of this disconnection through cross-material comparative analysis and translate it into concrete research gaps and a future roadmap.

5. Cross-material Comparative Analysis, Research Gaps, and Future Perspectives

5.1. A New Mechanistic Classification Framework for Anisotropy Origins

Building on the systematic review of all three material systems, a mechanistic anisotropy classification framework is proposed. Unlike existing literature that typically describes AM material anisotropy by build orientation (horizontal/vertical) [8,10,13], the present mechanistic framework explains why different materials respond so differently to heat treatment, carrying direct implications for JC calibration strategy selection.

- Texture-precipitate coupling type (IN718): Anisotropy is jointly governed by <001> fiber texture of columnar gamma grains and heterogeneous interdendritic Laves phase distribution. Heat treatment substantially reduces anisotropy through Laves phase dissolution and promoted homogeneous precipitation (YS directional difference reduced from ~15% to < 5% [10,22]). Characteristic: anisotropy is 'controllable' with heat treatment as the primary lever; anisotropy affects both A and n parameters, exerting the most comprehensive influence on the JC parameter system.
- Grain boundary-texture type (TC4): Anisotropy originates from the orientation consistency of Widmanstatten alpha lamellae and the continuity of GB-alpha films (> 70% grain boundary coverage [8]). Achieving isotropy requires microstructural transformation; conventional annealing is largely ineffective [8,15]. Characteristic: anisotropy is primarily expressed in elongation rather than YS, and is 'difficult to eliminate by conventional annealing'; directional influence falls mainly on n and C parameters with smaller A directional differences.
- Phase distribution-thermal history type (18Ni300): Anisotropy is controlled by non-uniform in-situ aging precipitate distribution (gradient aging) and delta-ferrite distribution, with the primary direction being a build-height gradient rather than in-plane directional differences (< 5% [13,37,38]). Characteristic: the most distinctive anisotropy type; SLM/LPBF data show directional A differences of ~13.7% [12,13], while WAAM gradient effects (~15% [37]) may be even more pronounced — the most complex and difficult-to-standardize anisotropy mechanism among the three materials.

5.2. JC Parameter Directional Sensitivity and Three-tier Error Priority

Based on the data in **Table 2**, the directional sensitivity ranking of JC parameters across the three material systems is as follows: A parameter is most sensitive to anisotropy — 18Ni300 directional difference ~13.7% (0°: A = 816.72, 90°: A = 705 [12]); IN718 directional difference 5-15% (< 5% after heat treatment [10]); TC4 directional difference ~10% (from TC11 reference [54]). The n parameter shows significant directional variation in 18Ni300 (0°: n = 0.303, 90°: n = 0.209, ~31% difference [13]), with < 10% directional differences in IN718 and TC4. Directional C data are most scarce — TC11 data [54] imply ~25% directional C difference, while IN718 and 18Ni300 lack systematic data, representing one of the most severe current data gaps. The m parameter shows essentially no reported anisotropy across all three materials, constituting another important research void.

Based on the data in **Table 2**, the three-tier error magnitudes for WAAM IN718 can be quantified as follows. Xi et al. [9] reported a heat-treated JC parameter A = 1025.4 MPa alongside an as-deposited quasi-static YS of approximately 597 MPa for the same material [9], yielding a state-jump error of $\delta\_state = |1025.4 - 597|/597 \approx 42\%$. The anisotropy error, assessed using the most comprehensive directional dataset available (18Ni300 inverse identification by Eisseler et al. [12]), amounts to $\delta\_aniso = |816.72 - 705|/761 \approx 14.6\%$. After rigorous modified-JC calibration, the residual model error is $\delta\_model < 1.71\%$ [9]. The resulting priority hierarchy — δ_state (42%) substantially exceeds δ_aniso (14.6%) substantially exceeds δ_model (<2%) — has a direct engineering implication: establishing as-deposited-specific parameter sets yields an order-of-magnitude larger accuracy gain than refining the JC functional form.

Figure 5 translates the quantitative analysis of this section into graphical form. Panel (a) is an original grouped bar chart comparing the directional differences of JC parameters A, n, and C across the three WAAM material

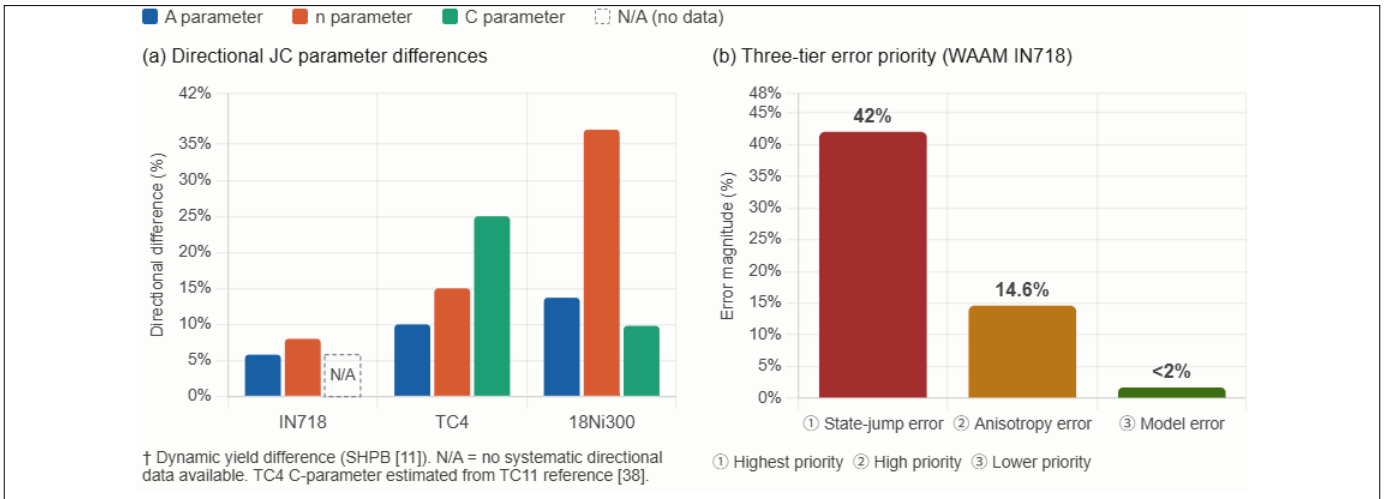

Figure 5. (a) Directional differences (%) of JC parameters A, n, C for WAAM IN718 [9,18], TC4 [38], and 18Ni300 [10,11]. TC4 C-parameter (~25%) estimated from TC11 (Ti-6.5Al-3.5Mo) reference data [38]; direct WAAM TC4 C-direction data unavailable. N/A = no systematic directional data available. (b) Three-tier error priority for WAAM IN718: δ_{state} = 42% [8,9] substantially exceeds δ_{aniso} = 14.6% [10] substantially exceeds δ_{model} <2% [8]. Data from **Tables 1–2**.

systems, compiled from **Table 2**. Among the three materials, 18Ni300 exhibits the largest A-parameter directional difference (approximately 13.7%, from Eisseler et al. [10]) and the largest n-parameter directional difference (approximately 37%, from Liang et al. [11]); IN718 shows intermediate A and n differences (5–15% and ~8%, respectively [9,18]); TC4 shows the smallest A-parameter difference but the largest C-parameter directional variation (approximately 25%, estimated from TC11 reference data [38]). The absence of systematic directional C data for IN718 and 18Ni300 (marked N/A) directly reinforces Gap 4 identified in Section 5.3. Panel (b) is an original waterfall bar chart presenting the three-tier error priority hierarchy for WAAM IN718, making immediately apparent the large disparity between state-jump error (δ_state = 42% [8,9]), anisotropy error (δ_aniso = 14.6% [10]), and model calibration error (δ_model < 2% [8]). The order-of-magnitude differences between tiers justify the priority sequence proposed in this review: establishing as-deposited-specific parameter sets first, resolving directional parameterization second, and improving JC functional form third.

This three-tier priority analysis yields a critical engineering resource allocation insight: improving the JC functional form contributes at most ~3 percentage points to accuracy (reducing model error from ~5% to <2%), whereas establishing as-deposited-specific parameter sets eliminates ~42% state-jump error — a 14-fold greater benefit. Behseresht and Park [63] provided supplementary validation from a process simulation perspective: JC model reduces warpage prediction error from ~20% to ~8% compared to isotropic hardening models, confirming that even in process simulation contexts, accurate thermal softening description carries significant precision benefits [63]. Okuniewski et al. [51] corroborated the breadth of printing-direction effects from a different material system: WLMD 316L shows A difference of 26% and n difference of 169% between 0° and 90° printing directions [51].

5.3. Literature Coverage Matrix and Five Core Research Gaps

The cross-material comparative analysis directly implies a systematic gap between existing literature coverage and engineering requirements. Analysis through a 'literature coverage matrix' (rows: material x state; columns: A/B/n/C/m parameters x directional coverage) reveals that the most poorly covered dimension is the thermal softening exponent m — WAAM as-deposited m values are entirely absent for all three materials, with all existing measurements from wrought stock, directly limiting simulation fidelity for WAAM components in extreme high-temperature service. Five prioritized research gaps are identified:

Highest priority: Complete five-parameter JC data absence for WAAM as-deposited 18Ni300 [12-14,37]. No study has yet simultaneously covered quasi-static, dynamic, and elevated-temperature JC calibration for WAAM as-deposited 18Ni300. The combination of low n (~0.2), gradient aging effects, and delta-ferrite soft inclusions makes this the most scientifically challenging and engineering-critical calibration task — this alloy grade is already widely deployed in aerospace tooling and high-pressure structural components fabricated by WAAM, and the absence of constitutive data directly constrains reliability design.

High priority: Absence of WAAM TC4 as-deposited JC data [8,33,36,54] and systematic m parameter gap across all three material systems [1,52,56]. Despite TC4 being one of the most studied materials in WAAM, comprehensive JC calibration for as-deposited Widmanstatten microstructure is nearly absent, with TC11 work [54] providing methodological reference but non-transferable parameters. TC4 WAAM as-deposited components are already widely used in as-deposited (heat-treatment-free) aerospace applications, making this gap highly urgent. The m parameter gap affects extreme high-temperature service simulation for all three material systems.

Medium priority: Scarcity of directional JC parameter sets and non-standardized accuracy evaluation criteria. Studies providing DD and SD directional parameter sets are extremely rare (18Ni300: only 2 studies [12,13]; IN718 and TC4 as-deposited: none). Non-uniform reporting of accuracy metrics (AARE, R^2, maximum error) [7,9,11,54,56] prevents cross-literature benchmarking, necessitating a unified WAAM material JC parameter accuracy evaluation protocol. The absence of predictive models quantitatively linking microstructural parameters to JC parameters [44,65] is a deep-seated methodological barrier to forward design workflows.

5.4. Three Technical Challenges

Advancing the above gap-filling research faces three primary technical challenges differing substantially in difficulty and solution pathways. High-temperature SHPB precision is the core obstacle to obtaining m parameters. At temperatures above 1000 °C, radiative heat loss (heat flux density > 10^4 W/m^2) and bar oxidation substantially increase stress wave analysis errors, requiring purpose-designed tungsten-rhenium alloy bars and vacuum/atmosphere protection systems [52,54]. This challenge is most severe for IN718 — the temperature range required to fully characterize DSA behavior (400-800 °C) overlaps with the reliable operating range of high-temperature SHPB systems, making error source separation extremely difficult and explaining why m remains unreported for WAAM IN718 [9,25].

Small-specimen size effects originate from WAAM's layer-by-layer geometry: deposition layer thickness typically 1-3 mm constrains SHPB specimen diameter to typically < 5 mm when extracting from specific height positions. When specimen diameter to grain size ratio < 10, statistical representativeness is insufficient and single-grain orientation effects dominate [33,54]. IN718 columnar grain widths can reach 1-3 mm and TC4 prior-beta grain widths 0.5-2 mm, both potentially introducing systematic directional biases in small specimens; developing dedicated size-effect correction protocols is an important near-term methodological research objective. The 18Ni300 low-n fitting stability challenge is the most material-specific: with n approximately 0.2, power-law fitting is extremely sensitive to the yield point definition, with 0.2% vs 0.1% offset conditions yielding A values differing by ~50 MPa (~6% [13,14]). Introducing Voce hardening law constraints and Bootstrap resampling uncertainty quantification provides a viable methodological solution [14].

5.5. Future Research Roadmap

5.5.1. Near-term (1-3 Years): As-deposited Parameter Database Construction

The near-term research priority is to fill the two most critical parameter gaps. For WAAM as-deposited TC4, a systematic experimental matrix is recommended: quasi-static stage at 0.001, 0.01, 0.1 s^{-1} x 25, 200, 400, 600, 800 °C (15 test conditions); dynamic stage at 500, 1000, 2000, 3000 s^{-1} x 25 °C (4 conditions); high-temperature dynamic stage at 1000 s^{-1} x 400, 600 °C (2 supplementary conditions); totaling 21 test points. This matrix maintains comparable strain rate span and temperature coverage with Tian et al.'s TC11 testing design [54], ensuring direct cross-alloy benchmarking. Notably, TC11 (Ti-6.5Al-3.5Mo) and TC4 (Ti-6Al-4V) differ in quasi-static YS by approximately 120-180 MPa [30,54], so TC11's temperature-point selection logic and strain rate span design can be directly borrowed, but absolute parameter values must be independently obtained for TC4. Both DD and SD directions should be simultaneously calibrated to achieve the first systematic quantification of directional JC parameters for WAAM TC4 [8].

For WAAM as-deposited 18Ni300, a two-phase approach is recommended. Phase 1 (quasi-static): 0.001 s^{-1} x 25-600 °C, 6 test conditions, focusing on low-n fitting stability via Voce law constraints and Bootstrap uncertainty quantification to determine A, B, n parameters with confidence intervals [13,14]. Phase 2 (dynamic): 1000 and 2000 s^{-1} x 25 °C, 2 SHPB conditions, with simultaneous adiabatic temperature rise iterative correction [53]. This plan requires only 8 experimental conditions total, establishing the world's first WAAM as-deposited 18Ni300 JC reference parameter set with minimum experimental resources, directly filling the most critical literature gap.

5.5.2. Mid-term (3-5 Years): Microstructure-Parameter Models and Calibration Standardization

Mid-term research should deepen in two directions based on near-term data accumulation. The construction of microstructure-JC parameter correlation predictive models targets WAAM IN718 as the first breakthrough. Based on the Orowan precipitation strengthening mechanism [66], parameter A can be approximated as the sum of matrix strength and precipitation strengthening increment:

$$A \approx \sigma_{\text{matrix}} + \frac{0.4\mu bM}{\pi\lambda} \ln\left(\frac{2\,\bar{r}}{b}\right) \quad (2)$$

where μ is the matrix shear modulus, b is the Burgers vector, M is the Taylor factor, λ is the inter-precipitate spacing, and $\bar{r}$ is the mean precipitate radius.

Correlating EBSD data (texture and grain information) and TEM data (precipitate volume fraction and size) across different heat treatment states with JC parameter A values can construct a quantitative model for directly predicting A from microstructural parameters, targeting a prediction error < 8% [44,65]. Once established, this model substantially reduces the need for repeated calibration across different heat treatment states — particularly valuable for engineering applications requiring coverage of multiple microstructural states.

Regarding anisotropic constitutive calibration standardization, the Hill48-JC coupling framework describes orthotropic anisotropy through six anisotropy coefficients (F, G, H, L, M, N), decoupled in calibration from the JC flow stress equation, representing the optimal minimal-complexity solution for handling WAAM textural anisotropy. Based on estimates from Okuniewski et al.'s 316L data [51], the Hill48-JC coupled model improves prediction accuracy

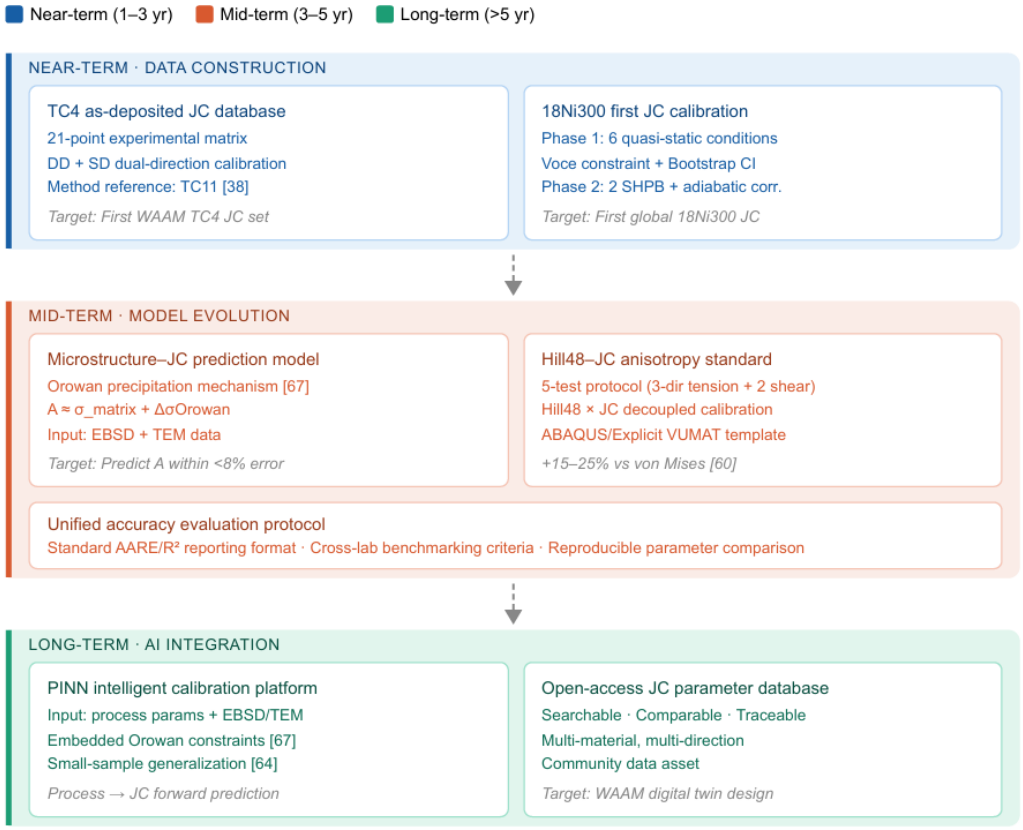

Figure 6. Research roadmap for WAAM constitutive modeling.

by approximately 15-25% compared to the von Mises assumption when directional strength differences exceed 10%. Standardized five-test protocols (3-direction uniaxial tension + 2-direction shear) should be developed alongside VUMAT subroutine templates compatible with ABAQUS/Explicit [12,13].

5.5.3. Long-term (>5 Years): AI-assisted Intelligent Calibration Platform

The expanding scope of metal additive manufacturing applications across medicine, aerospace, and industrial sectors [67] underscores the growing need for reliable constitutive parameter databases that can scale with this technological proliferation. Zhang et al. [67] highlighted that machine learning will play an increasingly central role in quality control for metal AM components — a vision that inherently depends on robust, materials-specific constitutive data as foundational inputs. This further reinforces the urgency of the near-term database-building activities proposed in this roadmap.

Building on the multi-material, multi-directional JC parameter database established in near- and mid-term research, the long-term goal is to construct an AI-assisted WAAM material constitutive intelligent calibration platform. Physics-informed neural networks (PINN [68]) take WAAM process parameters (heat input Q = UI/v, inter-layer temperature, cooling rate) and microstructural features (grain size, precipitate volume fraction, GB-alpha thickness) as inputs and JC parameter sets as outputs, while embedding physical constraints (Orowan strengthening equation [66], thermodynamic phase transformation equations) in the loss function to maintain physical consistency under limited data availability. Compared to purely data-driven neural networks, PINN demonstrates superior generalization under small-sample conditions [68], better suited to the data-scarce reality of WAAM constitutive research.

The long-term objective is to establish an open-access WAAM material constitutive database platform, consolidating the currently scattered literature parameters into searchable, comparable, and traceable standardized data assets — advancing WAAM component constitutive modeling from its current fragmented, literature-by-literature paradigm toward a systematic, cumulative scientific framework that fundamentally elevates the reliability of WAAM component digital design [5,68].

Figure 6 presents the proposed research roadmap as a three-tier vertical flow diagram organized by time horizon. The near-term data construction tier (blue, 1–3 years) addresses the two highest-priority gaps identified in Section 5.3: a TC4 as-deposited JC database via a 21-point experimental matrix (quasi-static: 15 conditions; dynamic: 4 conditions; high-temperature dynamic: 2 conditions), and the world's first WAAM as-deposited 18Ni300 JC calibration via an 8-condition two-phase protocol (Phase 1: 6 quasi-static conditions with Voce constraint and Bootstrap uncertainty quantification; Phase 2: 2 SHPB conditions with adiabatic temperature rise correction [39]). The mid-term model evolution tier (orange, 3–5 years) builds upon the near-term database in two parallel directions: an Orowan-mechanism-based microstructure–JC parameter prediction model targeting A-value prediction error below 8% [67], and a Hill48–JC anisotropic coupling calibration standard with an accompanying ABAQUS/Explicit VUMAT subroutine template [10,11,60], alongside a unified accuracy evaluation protocol to enable cross-laboratory benchmarking. The long-term AI integration tier (green, >5 years) culminates in a Physics-Informed Neural Network (PINN)-based [64] intelligent calibration platform — taking WAAM process parameters and microstructural features as inputs and JC parameter sets as outputs, with Orowan constraints embedded in the loss function — feeding into an open-access, searchable parameter database that enables full WAAM component digital twin design. Dashed arrows between tiers indicate prerequisite dependencies: near-term data are required before mid-term models can be validated, and both are needed before the AI platform can achieve meaningful cross-material generalization.

Looking further ahead, the AM technology landscape continues to diversify across scales; advances in nano-level additive manufacturing processes [69] may eventually inspire new thinking in microstructure-tailored deposition strategies for macro-scale WAAM, though the bridging mechanisms remain an open research question.

6. Conclusions

This review systematically examined the tensile behavior and JC constitutive calibration progress for WAAM-fabricated IN718, TC4, and 18Ni300 across 69 representative publications, yielding the following regulatory conclusions:

(1) The non-equilibrium solidification characteristics of WAAM render material anisotropy unavoidable across all three systems, with the primary manifestation mode determined by the phase transformation pathway: IN718 is texture-precipitate coupling type (heat-treatment-controllable, YS directional difference reduced from 15% to <5% [10,22]); TC4 is grain boundary-texture type (difficult to eliminate by conventional annealing [8,15]); 18Ni300 is phase distribution-thermal history type (primary direction is a build-height gradient

rather than in-plane directional difference [37]). This taxonomy reveals the physical basis for adopting different JC modeling strategies for each material system.

(2) Quantitative analysis establishes a three-tier error priority: state-jump error (as-deposited to heat-treated, ~42% [9,10]) substantially exceeds anisotropy error (~14.6% [12,13]) substantially exceeds rigorous calibration model error (<2% [9]). The engineering implication is that establishing as-deposited-specific parameter sets is the highest-priority action for improving WAAM component simulation fidelity, with contributions far exceeding improvements to JC functional form.

(3) The systematic errors of classical JC (10-30%) for WAAM materials at high strain rates (>1000 s-1) and elevated temperatures (>600 °C) have definitive physical origins: DSA/PLC effect in IN718 (Nb concentration 2-3x higher than wrought, expanding PLC window [25]); alpha-to-beta phase transformation softening inflection in TC4 (500-600 °C [35,52]); TRIP effect in 18Ni300 — all three mechanisms exceed classical JC's descriptive capacity. Temperature-strain rate coupling correction [9,11], adiabatic temperature rise iterative correction [53], and anisotropic parameterization [12,13] represent the three core improvement directions.

(4) JC calibration for WAAM IN718 has made preliminary progress: modified JC achieves AARE < 1.71% for heat-treated IN718 [9] (recommended, ★ symbol); WAAM TC4 as-deposited JC calibration is nearly absent, with wrought parameter transplantation error ~8% (estimated from TC11 comparison [54]); all five JC parameters for WAAM as-deposited 18Ni300 remain entirely uncharacterized, the most critical gap across the three material systems [12-14,37].

(5) The thermal softening exponent m is systematically absent for all three WAAM material systems — the most neglected parameter gap: IN718 exhibits non-monotonic behavior due to DSA effects [9,25]; TC4 shows a phase-transformation-induced inflection at 500-600 °C [35,52]; 18Ni300 has zero m data reported. m-value absence directly limits simulation fidelity in high-temperature WAAM service scenarios and should be incorporated into near-term experimental planning.

(6) The future research roadmap is: near-term (1-3 years) — establish WAAM as-deposited TC4 and 18Ni300 JC parameter databases (21+8 experimental matrices detailed in Section 5.5 [7,53,54]); mid-term (3-5 years) — develop Orowan-mechanism-based microstructure-JC parameter correlation models [65,66] and Hill48-JC anisotropic coupling calibration standards [12,13,51]; long-term (>5 years) — construct a PINN-based WAAM constitutive intelligent calibration platform [67,68].

Acknowledgements

This work was supported by Shandong Agriculture and Engineering University Start-Up Fund for Talented Scholars (BSQJ-202301), and Youth Fund of Shandong Agriculture and Engineering University (QNKJZ202301).

Conflicts of Interest

The authors declare that the research was conducted in the absence of any commercial or financial relationships that could be construed as a potential conflict of interest.

References

[1] G. R. Johnson, W. H. Cook. "A constitutive model and data for metals subjected to large strains, high strain rates and high temperatures." *Proc. 7th Int. Symp. Ballist.* **1983**, *21*, 541-547.

[2] S. W. Williams, F. Martina, A. C. Addison, J. Ding, G. Pardal, P. Colegrove. "Wire + arc additive manufacturing." *Mater. Sci. Technol.* **2016**, *32*, 7, 641-647.

[3] L. Vazquez, M. N. Rodriguez, I. Rodriguez, P. Alvarez. "Influence of Post-Deposition Heat Treatments on the Microstructure and Tensile Properties of Ti-6Al-4V Parts Manufactured by CMT-WAAM." *Metals* **2021**, *11*, 8, 1161.

[4] X. A. Jimenez, J. Song, Y. Fu, A. C. To. "Ensuring Melt Track Width Consistency and Crack-Free Conditions Using Interpass-Temperature-Dependent Process Parameters for Wire-Arc-Directed Energy-Deposited Inconel 718." *Journal of Manufacturing and Materials Processing*.**2024**, *8*, 4, 140.

[5] J. Ding, P. Colegrove, J. Mehnen, S. Ganguly, P. M. Sequeira Almeida, F. Wang, S. Williams. "Thermo-mechanical analysis of wire and arc additive layer manufacturing process on large multi-layer parts." *COMP.MATER. SCI.***2011**, *50*, 12, 3315-3322.

[6] B. Das, S. S. Roy, A. Tripathi, P. Bhatt, S. Vasudevan, S. Velu. "WAAM: A comprehensive review of process, materials, modelling, artificial intelligence, and industrial applications." *J. ALLOY.COMPD.***2026**, *1058*, 176523.

[7] Y. Fan, B. Wang, Z. Hao. "Study on dynamic mechanical properties and constitutive model description of Inconel718." *P.I MECH ENG.C-J. MEC.***2022**, *236*, 10, 5495-5509.

[8] L. Gambirasio, E. Rizzi. "On the calibration strategies of the Johnson-Cook strength model: discussion and applications to experimental data."*MAT. SCI ENG.A-STRUCT.***2014**, *610*, 370-413.

[9] B. E. Carroll, T. A. Palmer, A. M. Beese. "Anisotropic tensile behavior of Ti-6Al-4V components fabricated with directed energy deposition additive manufacturing." *Acta.Mater.* **2015**, *87*, 309-320.

[10] N. Xi, J. Tang, J. Li, T. Jiang, C. Tan. "Wire arc additive manufacturing of Inconel 718: constitutive modelling and its microstructure basis."*J.MANUF. PROCESS.***2022**, *75*, 1134-1143.

[11] C. E. Seow, H. E. Coules, G. Wu, R. H. U. Khan, X. Xu, S. Williams. "Wire + arc additively manufactured Inconel 718: effect of post-deposition heat treatments on microstructure and tensile properties." *Mater.Des.***2019**, *183*, 108157.

[12] R. Eisseler, D. Gutsche, C. Maucher, H. C. Mohring. "Inverse determination of Johnson-Cook parameters of additively produced anisotropic maraging steel." *Materials* **2022**, *15*, 1, 26.

[13] Z. Liang, Q. Zhang, W. Li, W. Li. "Research on the mechanical response and constitutive model of 18Ni300 manufactured by SLM with different build directions." *Materials* **2024**, *17*, 17, 4246.

[14] T. E. F. Silva, A. V. L. Gregorio, A. Reis, P. A. F. Martins. "Modelling of 18Ni300 additively manufactured steel under extreme loading conditions for predictive analytical purposes."*JMMP.***2021**, *5*, 4, 114.

[15] P. A. Colegrove, H. E. Coules, J. Fairman, F. Martina, T. Kashoob, H. Mamash, L. D. Cozzolino. "Microstructure and residual stress improvement in wire and arc additively manufactured parts through high-pressure rolling."*J. Mater. Process. Technol.***2013**, *213*, 10, 1782-1791.

[16] D. Panov, G. Permyakov, S. Naumov, V. Mirontsov, E. Kudryavtsev, L. Sun, et al. "The Effect of Post-Deposition Heat Treatment on the Microstructure, Texture, and Mechanical Properties of Inconel 718 Produced by Hybrid Wire-Arc Additive Manufacturing with Inter-Pass Forging." *Metals*.**2025**, *15*, 1, 78.

[17] D. Deng, J. Moverare, R. L. Peng, H. Soderberg. "Microstructure and anisotropic mechanical properties of EBM manufactured Inconel 718 and effects of post heat treatments."*Mater. Sci. Eng. A.***2017**, *693*, 151-163.

[18] E. A. Tolcha, V. Sreenivasan, M. S. Anis, S. Ganguly, J. Ding, S. Williams. "Thermodynamic and atomic diffusion behavior of WAAM Inconel 718 components."*J.ALLOY.COMPD.***2026**, *1058*, 176821.

[19] V. A. Popovich, E. V. Borisov, A. A. Popovich, V. Sh. Sufiiarov, D. V. Masaylo, L. Alzina. "Functionally graded Inconel 718 processed by additive manufacturing: crystallographic texture, anisotropy of microstructure and mechanical properties."*Mater. Des.***2017**, *114*, 441-449.

[20] X. Xu, J. Ding, S. Ganguly, C. Seow, S. Williams. "Investigation of process factors affecting mechanical properties of INCONEL 718 superalloy in wire + arc additive manufacture process." *J. Mater. Process. Technol.* **2019**, *265*, 201-209.

[21] O. Y. Smetannikov, P. V. Maksimov, Y. A. Koshkina, M. V. Krechetov. "Experimental study and numerical modeling of inter-pass forging in wire-arc additive manufacturing of Inconel 718." *Materials* **2026**, *19*, 1, 182.

[22] P. Kumar, S. K. Sharma, R. K. R. Singh. "Effect of cooling media on bead geometry, microstructure, and mechanical properties of wire arc additive manufactured IN718 alloy."*Adv. Manuf.***2024**, *12*, 1, 124-149.

[23] H. Qi, M. Azer, A. Ritter. "Studies of standard heat treatment effects on microstructure and mechanical properties of laser net shape manufactured INCONEL 718."*Metall. Mater. Trans.A.***2009**, *40*, 10, 2410-2422.

[24] T. Zhang, C. T. Liu, C. N. Sun, T. H. Goh, J. Wei, J. Bi, E. Liu. "Effect of rolling force on tensile properties of additively manufactured Inconel 718 at ambient and elevated temperatures."*J ALLOY COMPD.***2021**, *884*, 161163.

[25] W. S. James, S. G. Kott, M. H. Koul, A. Haney, L. T. Williams. "High temperature performance of wire arc additively manufactured Inconel 718."*Sci. Rep.***2023**, *13*, 22685.

[26] R. H. Song, X. Zhang, Y. J. Yang, H. L. Zheng, X. H. Li. "High-temperature mechanical properties and the Portevin-Le Chatelier effect for wire arc additively manufactured Inconel 718 superalloy." *Metals* **2025**, *15*, 9, 949.

[27] T. Bhujangrao, F. Veiga, A. Suarez, E. Iriondo, F. G. Mata. "High-temperature mechanical properties of IN718 alloy: comparison of wrought and wire arc additive manufacturing (WAAM) samples." *Crystals* **2020**, *10*, 9, 689.

[28] T. Zhang, C. T. Liu, K. Li, C. N. Sun, J. Wei. "Hybrid WAAM and effect

of rolling on microstructure, texture and properties of Inconel 718."*J.Manuf. Process*.**2022**, *299*, 105069.
[29] U. Alonso, F. Veiga, A. Suarez, T. Artaza. "Characterization of Inconel 718 nickel-base superalloy manufactured by wire arc additive manufacturing: effect on mechanical properties and machinability."*J. Mater.Sci.Technol*.**2021**, *14*, 2665-2676.
[30] E. Brandl, A. Schoberth, C. Leyens. "Morphology, microstructure, and hardness of titanium (Ti-6Al-4V) blocks deposited by wire-feed additive layer manufacturing (ALM)."*Mater. Sci. Eng. A*.**2012**, *532*, 295-307.
[31] B. A. Szost, S. Terzi, F. Martina, D. Boisselier, A. Prytuliak, T. Pirling, M. Hofmann, D. J. Jarvis. "A comparative study of additive manufacturing techniques: residual stress and microstructural analysis of CLAD and WAAM printed Ti-6Al-4V components."*Mater. Des.***2016**, *89*, 559-567.
[32] S. Zhou, J. Zhang, G. Yang, Z. Li, D. Pan. "Microstructure evolution and fracture behavior of Ti-6Al-4V fabricated by WAAM-LDM additive manufacturing."*J.Mater.Sci.Technol*.**2024**, *28*, 347-362.
[33] L. Ji, J. Lu, S. Tang, Q. Wu, J. Wang, H. Han, M. Ma. "Research on mechanisms and controlling methods of macro defects in TC4 alloy fabricated by wire additive manufacturing." *Materials* **2018**, *11*, 7, 1104.
[34] H. Wu, S. Cai, C. Li, L. Zhao, J. Ding. "High-temperature strength and microstructural evolution of Ti-6Al-4V alloy fabricated by WAAM under elevated temperature."*Sci. Rep*.**2025**, *15*, 31895.
[35] J. Wang, H. Wang, T. Xu, Z. Li, C. Liu. "Research on the microstructure and mechanical properties of functional gradient materials of TC4/TC11 titanium alloys for wire arc additive manufacturing with different transitional forms."*J.Manuf.Process.***2024**, *131*, 245-255.
[36] S. Kim, D. H. Kam, K. A. Lee. "Characterization of the microstructure and mechanical properties of Ti-6Al-4V alloy fabricated by wire-arc additive manufacturing."*Sci. Rep.***2025**, *15*, 31895.
[37] X. Xu, S. Ganguly, J. Ding, C. E. Seow, S. Williams. "Microstructural evolution and mechanical properties of maraging steel produced by wire + arc additive manufacture process."*Mater. Charact.***2018**, *143*, 152-162.
[38] C. D. Mota, A. A. Ferreira, A. B. Moreira, P. M. G. P. Moreira, J. P. Oliveira. "Wire-laser additive manufacturing of Inconel 718 claddings on S355 and 304L steels: process window and heat treatment optimization."*MACHINES.***2026**, *14*, 281.
[39] M. Pan, J. Xu, N. Liang, Y. Zou, Y. Zhao. "Microstructure and mechanical properties of the laminated heterostructured material with 316L stainless steel/18Ni300 maraging steel fabricated by WAAM."*Mater. Sci. Eng. A*.**2023**, *881*, 145300.
[40] J. Zhang, J. Fan, J. Xu, D. Yang, Y. Peng, K. Wang. "The effect of heat input on the microstructure and mechanical properties of 18Ni 300 maraging steel fabricated by arc directed energy deposition."*Mater. Sci. Eng. A*.**2023**, *884*, 145545.
[41] J. Zhang, J. Fan, D. Yang, K. Wang, Y. Peng. "The fracture toughness and fatigue crack growth properties of 18Ni 300 maraging steel manufactured by wire + arc additive manufacturing."*Mater. Sci. Eng. A*.**2024**, *892*, 145993.
[42] M. Osman, S. Sarafan, P. Wanjara, J. Gholipour, N. Brodusch, R. Gauvin, M. Brochu. "Effect of heat treatment on the microstructure and mechanical properties of 18Ni-300 maraging steel produced by additive-subtractive hybrid manufacturing." *Materials* **2023**, *16*, 13, 4749.
[43] S. Sohail, B. C. M. Reddy. "Optimizing surface roughness and tool wear in MQL milling of 18Ni300 maraging steel."*Eng. Res. Express.***2025**, *7*, 025518.
[44] Z. Mao, X. Lu, H. Yang, X. Niu, L. Zhang, X. Shang. "Processing optimization, microstructure, mechanical properties and nanoprecipitation behavior of 18Ni300 maraging steel in selective laser melting."*Mater. Sci. Eng. A*.**2022**, *830*, 142334.
[45] S. Afkhami, K. Lipianen, V. Javaheri, T. Bjork. "Anisotropic mechanical behavior of L-PBF maraging steel under static and cyclic loading."*Mater. Sci. Eng. A*.**2023**, *876*, 145165.
[46] D. Peng, V. K. Champagne, A. S. Ang, A. Birt, A. Michelson, S. Pinches, R. Jones. "Computing the Durability of WAAM 18Ni-250 Maraging Steel Specimens with Surface Breaking Porosity." *Crystals* **2023**, *13*, 3, 443.
[47] M. Kishore, M. Srivastava, I. S. Raut. "Process optimization using response surface methodology for wire arc additive manufacturing of Inconel 718."*Adv. Manuf.***2026**.
[48] F. Martina, J. Mehnen, S. W. Williams, P. Colegrove, F. Wang. "Investigation of the benefits of plasma deposition for the additive layer manufacture of Ti-6Al-4V."*J. Mater. Process. Technol.***2012**, *212*, 6, 1377-1386.
[49] G. Asala, J. Andersson, O. A. Ojo. "Analysis and constitutive modelling of high strain rate deformation behaviour of wire–arc additive-manufactured ATI 718Plus superalloy."*INT.J.ADV .MANUF.TECH*.**2019**, *103*, 1, 1419-1431.
[50] G. Kishor, K. K. Mugada, R. P. Mahto, N. Bharat. "Constitutive modeling of high-temperature deformation, fracture mechanisms, and metallurgical study of WAAM-deposited Inconel 625 alloy."*Eng. Fail. Anal.* **2025**, *171*, 109350.
[51] W. Okuniewski, M. Walczak, M. Szala, D. Chocyk. "Johnson-Cook model depending on printing direction."*ADV.SCI.TECHNOL-RES*.**2026**, *20*, 2, 470-479.
[52] W. S. Lee, C. F. Lin. "High-temperature deformation behavior of Ti-6Al-4V alloy evaluated by high strain-rate compression tests."*J. Mater. Process. Technol*.**1997**, *75*, 1-3, 127-136.
[53] S. Zhu, J. Liu, X. Deng. "Modification of strain rate strengthening coefficient for Johnson-Cook constitutive model of Ti6Al4V alloy."*MATER. TODAY.COMMUN*.**2021**, *26*, 102016.
[54] Z. Tian, H. Wu, C. Tan, B. Luo, Y. Mao. "Dynamic mechanical properties of TC11 titanium alloys fabricated by wire arc additive manufacturing." *Materials* **2022**, *15*, 11, 3917.
[55] A. Muiruri, M. Maringa, W. du Preez. "Numerical simulation of high strain rate and temperature properties of LPBF Ti6Al4V(ELI) determined using a split Hopkinson pressure bar." *Materials* **2022**, *15*, 5, 1872.
[56] W. Grzesik, K. Zak, R. Chudy. "Determination of material constitutive laws for Inconel 718 superalloy under different strain rates and working temperatures."*J.MATER ENG.PERFORM*.**2017**, *26*, 5705-5714.
[57] M. A. Aslam, K. Zhang, S. B. Rayhan, M. Faizan, I. M. Bello. "An investigation of soft impacts on selected aerospace grade alloys based on Johnson-Cook Material Model."*J. Phys.:Conf. Ser.***2020**, *1707*, 012008.
[58] X. Tang, J. Xiang, K. Lu, Z. Li, G. Liu, D. Li. "Machining performance and surface quality of 18Ni300 maraging steel under surface active medium assistance."*J.Manuf.Process*.**2026**, *160*, 108715.
[59] X. Fu, J. Liao, C. Liu, X. Zhao, S. Li. "Fracture mechanism and model of 18Ni maraging steel."*SCI.TECHNOL.WELD.JOI*.**2020**, *25*, 4, 332-341.
[60] Y. Yao, X. Li, Y. He. "On the relations between specific cutting energy and tool wear in micro-cutting of 3J33 maraging steel."*INT.J.ADV.MANUF. TECH*.**2019**, *104*, 3123-3131.
[61] R. Raj, L. N. S. Chiu, A. Huang, D. Marla. "Analysing thermo-mechanical effects of in-situ micro-rolling in single-bead laser-directed energy deposition via finite element modelling."*Prog .Addit.Manuf*.**2024**, *10*, 6229-6248.
[62] R. Mathews, K. M. Nagaraja, R. Zhang, Y. Soderberg, J. Llorca. "Temporally continuous thermofluidic-thermomechanical modeling framework for metal additive manufacturing." *Procedia.CIRP*.**2024**, *121*, 180-185.
[63] S. Behseresht, Y. H. Park. "Warpage prediction in wire arc additive manufacturing: a comparative study of isotropic and Johnson-Cook plasticity models." *Metals* **2025**, *15*, 6, 665.
[64] S. Zhang, Z. Leng, Q. Duan, S. Zhao, Z. Li. "Experimental determination and simulation validation: Johnson-Cook model parameters and grinding simulation of 06Cr18Ni11Ti stainless steel welds." *Machines* **2024**, *12*, 9, 660.
[65] K. Yuan, X. Bai, Y. Gu, R. L. Peng, J. Moverare. "Physical constitutive model to describe the dynamic mechanical behavior of additively manufactured IN718 at a wide range of strain rates and temperatures."*INT. J.PLASTICITY*.**2021**, *136*, 102865.
[66] A. J. Ardell. "Precipitation hardening." *Metallurgical Transactions A* **1985**, *16*, 12, 2131-2165.
[67] Z. Zhang, H. Wang, J. Li, H. Fu. "Recent Applications of Metal Additive Manufacturing: A Review."*XDI*.**2025**, *1*, 1, 8.
[68] M. Raissi, P. Perdikaris, G. E. Karniadakis. "Physics-informed neural networks: a deep learning framework for solving forward and inverse problems involving nonlinear partial differential equations."*J. Comput. Phys*.**2019**, *378*, 686-707.
[69] I. Fidan, M. Alshaikh Ali, V. Naikwadi, S. Gudavasov, M. Mahmudov, M. Mohammadizadeh, Z. Zhang, A. Sharma. "Nano-level additive manufacturing: condensed review of processes, materials, and industrial applications." *Technologies* **2024**, *12*, 7, 117.